tion support the interpretation of the dynamics presented here (22).

REFERENCES AND NOTES

1. R. L. Fork et al., Opt. Lett. 12, 483 (1987).
2. C. V. Shank, Science 233, 1276 (1986).
3. For example, the photochemical dissociation of ICN has recently been probed with 100-fs optical pulses [M. Dantus, M. J. Rosker, A. H. Zewail, J. Chem. Phys. 87, 2395 (1987)].
4. C. H. Brito Cruz et al., Chem. Phys. Lett. 132, 341 (1986).
5. W. Stoeckenius and R. A. Bogomolni, Annu. Rev. Biochem. 51, 587 (1982).
6. S. O. Smith, J. Lugtenburg, R. A. Mathies, J. Membrane Biol. 85, 95 (1985).
7. R. R. Birge, Annu. Rev. Biophys. Bioeng. 10, 315 (1981).
8. M. L. Applebury et al., Biophysics J. 23, 375 (1978).
9. E. P. Ippen et al., Science 200, 1279 (1978).
10. M. C. Nuss et al., Chem. Phys. Lett. 117, 1 (1985).
11. A. V. Sharkov, A. V. Pakulev, S. V. Chekalin, Y. A. Matveetz, Biochim. Biophys. Acta 808, 94 (1985).
12. H.-J. Polland et al., Biophys. J. 49, 651 (1986).
13. J. W. Petrich et al., Chem. Phys. Lett. 137, 369 (1987).
14. A. G. Doukas et al., Proc. Natl. Acad. Sci. U.S.A. 81, 4790 (1984).
15. R. R. Birge and L. M. Hubbard, J. Am. Chem. Soc. 102, 2195 (1980).
16. A. B. Myers et al., J. Chem. Phys. 79, 603 (1983).
17. G. R. Loppnow and R. A. Mathies, Biophys. J., in press.
18. Because of the spectral evolution during the first 150 fs, it is questionable to extract simple first-order kinetic constants for the early processes with the absorbance data at just a single wavelength.
19. C. H. Brito Cruz et al., IEEE J. Quantum Elect. 24, 261 (1988).
20. W. T. Pollard et al., in preparation.
21. R. R. Birge, L. A. Findsen, B. M. Pierce, J. Am. Chem. Soc. 109, 5041 (1987).
22. J. Dobler et al., Chem. Phys. Lett., in press.

23. Supported by NIH grant GM 27057 and NSF grant CHE 86-15093.

12 January 1988; accepted 8 March 1988

The Nature of the Interior of Uranus Based on Studies of Planetary Ices at High Dynamic Pressure

W. J. Nellis, D. C. Hamilton, N. C. Holmes, H. B. Radousky, F. H. Ree, A. C. Mitchell, M. Nicol

Data from the Voyager II spacecraft showed that Uranus has a large magnetic field with geometry similar to an offset tilted dipole. To interpret the origin of the magnetic field, measurements were made of electrical conductivity and equation-of-state data of the planetary "ices" ammonia, methane, and "synthetic Uranus" at shock pressures and temperatures up to 75 gigapascals and 5000 K. These pressures and temperatures correspond to conditions at the depths at which the surface magnetic field is generated. Above 40 gigapascals the conductivities of synthetic Uranus, water, and ammonia plateau at about 20 (ohm-cm)$^{-1}$, providing an upper limit for the electrical conductivity used in kinematic or dynamo calculations. The nature of materials at the extreme conditions in the interior is discussed.

The Voyager II spacecraft data showed that Uranus has a strong magnetic field, which can be described approximately by a dipole of moment 0.23 G R_U^3, where R_U is the planetary radius (25,600 km). The dipole is centered at 0.3 R_U and its axis is tilted 60° from the axis of rotation. The maximum value at the surface is 1.1 G (1), twice the value for Earth, and the minimum surface value is 0.1 G. These unexpected and unusual Voyager data emphasize the need for laboratory measurements of planetary materials at interior conditions in order to derive planetary models consistent with the observational data. We report new shock-wave electrical conductivity and equation-of-state (EOS) data for planetary "ices" and for a liquid with an atomic composition representative of a mixture of the "ices." Our electrical conductivity data provide density and temperature dependences up to 75 GPa (0.75 Mbar) and 5000 K and provide an upper bound that can be used in kinematic and dynamo calculations to explain the magnetic field. Laboratory data and theory also allow us to hypothesize on the nature of the interior.

The composition of Uranus is estimated from the mass, radius, rotational rate, and gravitational field (2, 3). The combined magnetic-field and radio-emission data yielded an improved measurement of the rotation rate of 17.24 hours (4). This result led to improved values of the density moments, which are derived from the gravitational moments deduced from the observed precessions of the elliptical rings of Uranus. The density moments provide a constraint on the equations of state of candidate materials. Prior to Voyager II, Hubbard and MacFarlane proposed that Uranus consists of three layers: an outer gas layer of H_2-He; a middle "ice" layer composed mostly of H_2O, CH_4, and NH_3; and an inner rocky core (2). The "ices" are actually in the fluid phase over a substantial portion of these proposed thermodynamic conditions.

After Voyager II, Kirk and Stevenson proposed that the magnetic field and the density moments derived from improved values of the rotation rate and gravitational moments are consistent with a greater degree of material mixing (5) than in the pre-Voyager models. One model consists of an outer gas-ice-rock region, which is mostly an H_2O-H_2 mixture, and an inner rocky core. The boundary is at 0.3 R_U and 300 GPa and 6000 K. The magnetic field is produced primarily in an H_2O-rich region near 0.7 R_U at 50 to 100 GPa, based on a kinematic model that considers equatorial zonal jet flow and uses the electrical conductivity of water extrapolated from Holzapfel's (6) fit to static and shock data up to 10 GPa and 1300 K. The Voyager II data were used by Gudkova et al. (7) and they also found more mixing. Their three-layer model has an outer H_2-He-ice region, a middle ice-rock layer, and an inner rocky core. The outer-middle boundary at 0.71 R_U is at 30 GPa and 2700 K and the middle-core boundary at 0.14 R_U is at 600 GPa and 6800 K. Their two-layer model is ice-rock for radii less than 0.72 R_U at 25 GPa and 2600 K, with H_2-He-rock-ice being the remainder. The vari-

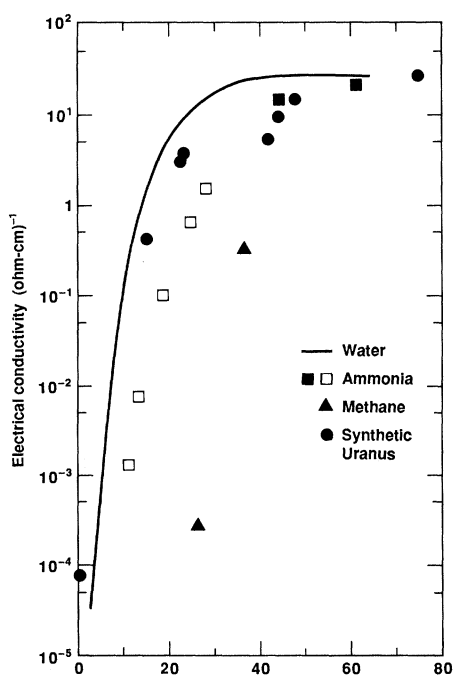

Fig. 1. Electrical conductivity versus shock pressure for planetary fluids. Solid symbols are the present work. Open squares are from (16). Solid curve is smooth curve through the data of (9) and (12). At 40 GPa, temperatures in these fluids are 2600 K in water, 2800 K in synthetic Uranus, 3100 K in ammonia, and 4100 K in methane.

W. J. Nellis, Physics Department and Institute of Geophysics and Planetary Physics, University of California, Lawrence Livermore National Laboratory, Livermore, CA 94550.
D. C. Hamilton, N. C. Holmes, H. B. Radousky, F. H. Ree, A. C. Mitchell, Physics Department, University of California, Lawrence Livermore National Laboratory, Livermore, CA 94550.
M. Nicol, Department of Chemistry and Biochemistry, University of California, Los Angeles, CA 90024.

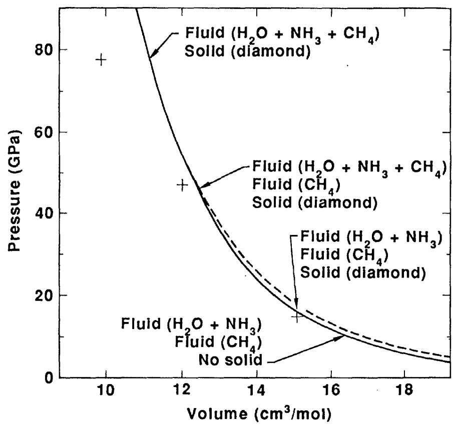

Fig. 2. Shock-compression equation of state of synthetic Uranus of initial density 0.896 g/cm^3 and initial temperature 295 K. Pluses are experimental points with error bars. Solid curve is theory with molecular-fluid phase separation; dashed curve is theory for a homogeneous fluid. Calculated equilibrium phases are indicated at four positions. At 76 GPa temperature is 5100 K.

ous models demonstrate that a unique model for Uranus is not yet possible. These models and the fact that the magnetic field is centered at 0.3 R_U, which means that the large surface magnetic field of 1.1 G is generated at even larger radii (~0.7 R_U), indicate that the most relevant conductivity data are in the range 10 to 100 GPa and several thousand degrees kelvin, the regime in which we have made our measurements.

Shock-wave EOS (*8–10*), temperature (*11*), electrical conductivity (*9, 12*), and spontaneous Raman scattering (*13*) data were measured for water up to the 100-GPa range. For ammonia (*9, 14*) and methane (*15*) EOS data have been obtained up to 70 and 90 GPa, respectively. Conductivities and temperatures of ammonia were measured up to 28 GPa (*16*) and 61 GPa (*17*), respectively. Shock data are relevant to planetary interiors because the shock compression of liquid specimens achieves the same high pressures and temperatures as the isentropic compression of low-density gas to form the giant planets (*18*).

We report here new electrical conductivity and shock temperature data for NH_3, CH_4, and the mixture we call "synthetic Uranus." EOS data were also measured for this mixture, an H-rich liquid with an H:O composition ratio of 3.5:1 and abundance ratios close to the cosmological ones of O:C (7:4) and O:N (7:1). It is a solution of water, ammonia, and isopropanol (C_3H_8O) with mole fractions of 0.71, 0.14, and 0.15, respectively. The H:O ratio is similar to that of the ice-gas mixture in the ratio 2.5:1 proposed for Uranus (*5*), assuming an H_2O-H_2 mix. High densities and temperatures achieved in shock experiments quickly induce chemical and thermal equilibrium, so that our results are expected to be weakly sensitive to the initial structure of the specimens. Although this mixture is not unique, we believe it is representative of a mixture of the planetary ices. Strong shock waves were generated by the impact of metal plates onto the front wall of liquid-specimen holders. The plates were accelerated up to 7 km/s by a two-stage light-gas gun. The experimental techniques were described previously (*9, 17*) and details are published elsewhere (*19*).

The electrical conductivities of shock-compressed liquid ammonia, methane, and synthetic Uranus are plotted versus shock pressure in Fig. 1. Previous data for water are included for comparison. The temperature measurements show that our conductivities are in the range 1500 to 5000 K. The electrical conductivities of synthetic Uranus, water, and ammonia all approach 20 (ohm-cm)$^{-1}$ above 40 GPa (*20*), providing an upper limit on the value of conductivity that can be used in kinematic or dynamo calculations. This limit is only weakly sensitive to chemical species. Below 40 GPa the conductivity of synthetic Uranus is a factor of 2 to 3 less than that of water. Shocked methane has substantially lower conductivity than the other fluids, at least up to 40 GPa and 4000 K, caused probably by the high stability of the CH_4 molecule. Thus, methane can only contribute to the magnetic field if it decomposes significantly into conducting phases at higher pressure and if the depths at which this occurs are sufficiently small so the field generated is significant at the surface.

The maximum conductivity can be used to characterize crudely the flow that produces the magnetic field. The dynamo theorem states that $R_M \equiv uR/\lambda \geq \pi^2$, where R_M is the magnetic Reynolds number, u is the maximum deviation of the velocity field from uniform rotation in a fluid sphere of radius R, $\lambda \equiv c^2/4\pi\sigma$ is the magnetic diffusivity, and σ is the electrical conductivity of the sphere (*21*). R_M is usually assumed to be in the range 10 to 100 for a steady external field. For $\sigma = 20$ (ohm-cm)$^{-1}$, $R = 0.7\,R_U$, and $R_M = 50$, then $u = 10^{-1}$ cm/s, which is small compared to the linear rotational velocity of 2×10^5 cm/s at 0.7 R_U.

Kirk and Stevenson showed that the magnitude of the magnetic field of Uranus can be calculated kinematically with the conductivity of water suppressed by a factor of 10. They assumed this factor to take account of dissolved insulating H_2-He (*5*). The conductivity of synthetic Uranus is still a factor of 3 to 5 larger than they used and allows for the presence of insulating phases. Thus, the shock-wave conductivity data for synthetic Uranus provide more representative experimental data than for pure water and this new data is consistent with the kinematic calculations of the magnetic field.

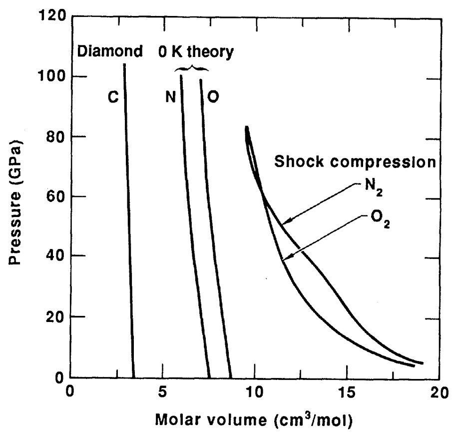

Fig. 3. Shock-compression equations of state for C (diamond) and liquid N_2 and O_2 and calculated 0 K isotherms for monatomic N and O, plotted as pressure versus molar volume. The 0 K curve for diamond is nearly the same as the shock-compression curve shown. The initial molar volumes of liquid N_2 and O_2 are 34.7 and 26.6 cm^3/mol, respectively.

Three EOS points were measured for synthetic Uranus and are plotted with chemical equilibrium calculations (*22*) for the shock-compression curve in Fig. 2. The calculation minimizes the free energy of the system with respect to nine molecular-fluid species and diamond. Equilibrium phases formed in the calculation are indicated at four locations on the shock-compression curve. The calculations suggest that at lowest shock pressures, the fluid separates into methane and ammonia-water phases. As pressure and temperature increase, diamond starts to form and methane becomes more soluble in the water-ammonia phase. The discrepancy between theory and experiment at highest pressures is probably caused by neglecting ionic species in the calculations, which cause the high electrical conductivities measured above 40 GPa.

The magnetic field and density moments, together with known material properties, provide evidence that Uranus is indeed composed of ice, gas, and rock. It is interesting to speculate on the nature of materials inside the planet. The high electrical conductivity of shocked water, the major ice constituent, is caused by molecular ionization (*12*). The same mechanism should apply to ammonia and synthetic Uranus. The range 10 to 20 GPa and 700 to 1200 K is an interesting one in which the ion concentration in H_2O increases from about 0.5% (*12*) to a saturation value, H bonds between H_2O molecules break (*13*), and the compressibility increases (*10*). Above 20 GPa water has been said to be totally ionized into OH^- and H_3O^+ (*12*). However, Raman scattering experiments at 26 GPa and 1700 K (*13*) show only a single broad O–H stretch band, which does not distinguish between vibrations in the H_2O molecule and OH^- ion. No indication of the H_3O^+ species is distinguishable in the spectra. Thus, the degree of dissociation of water cannot be determined from the Raman data. A lower bound on ion concentration can be estimated by assuming that mobile protons are the dominant charge carriers. By using a classical conductivity model and a mean free path of a molecular dimension, we estimate the proton concentration to be one proton for every ten original H_2O molecules at pressures above several tens of gigapascals. Thus, we estimate the degree of dissociation of water to be between 10 and 100% above 20 GPa and 1200 K.

At depths where the pressure exceeds 100 GPa and temperatures are several thousand degrees kelvin, molecules and ions are expected to dissociate and form dense, stiff monatomic or H–O–C–N species or both. This statement is based on observations of molecular dissociation at high shock pressures and temperatures. For example, N_2 starts to dissociate at only 30 GPa at 6000 K (*23*) but remains molecular to 130 GPa at 300 K (*24*), illustrating that high temperatures inside Uranus are expected to drive dissociation. Shock-compression curves for carbon (diamond) (*25*), nitrogen (*23*), and oxygen (*26*) and theoretical curves for monatomic simple-cubic N (*27*) and O (*28*) at 0 K are plotted as pressure versus volume in Fig. 3. The curves for the monatomic phases at 0 K are all steep; the shock-compression curves of liquid nitrogen and oxygen have comparable steep slopes above 60 GPa and 10,000 K. When dissociation is completed, intermolecular repulsion is replaced by stiffer interatomic repulsion. This transition is expected to proceed continuously along the planetary isentrope. In general, elements probably do not phase separate but form mixtures or react with each other to form compounds, which are nearly incompressible as in Fig. 3. Such materials might have high melting temperatures and condense out of the solution of the fluid "ice" mixture. Rock also has a stiff equation of state at high pressures. Thus, at pressures above 100 GPa planetary materials are probably close to their limiting compression, which contributes somewhat to the large volume of Uranus. That is, pressures above 100 GPa probably do not cause significant compression of the phases present because of their small compressibilities. Figure 3 suggests that all materials in the deep interior are dense, stiff materials having a high bulk modulus such as the diamond phase of carbon, which has been suggested to form inside Uranus (*29*).

REFERENCES AND NOTES

1. N. F. Ness *et al.*, *Science* **233**, 85 (1986).
2. W. B. Hubbard and J. M. MacFarlane, *J. Geophys. Res.* **85**, 225 (1980).
3. D. J. Stevenson, *Annu. Rev. Earth Planet. Sci.* **10**, 257 (1982).
4. M. D. Desch *et al.*, *Nature* **322**, 42 (1986).
5. R. L. Kirk and D. J. Stevenson, *Astrophys. J.* **316**, 836 (1987); D. J. Stevenson, *Bull. Am. Astron. Soc.* **19**, 851 (1987) and private communication.
6. W. B. Holzapfel, *J. Chem. Phys.* **50**, 4424 (1969).
7. T. V. Gudkova *et al.*, *Astron. Vestn.* (in Russian) **22**, 23 (1988).
8. J. M. Walsh and M. H. Rice, *J. Chem. Phys.* **26**, 815 (1957).
9. A. C. Mitchell and W. J. Nellis, *ibid.* **76**, 6273 (1982).
10. I. I. Sharipdzhanov *et al.*, *Combust. Explos. Shock Waves* (English translation) **19**, 668 (1984).
11. G. A. Lyzenga *et al.*, *J. Chem. Phys.* **76**, 6282 (1982).
12. H. G. David and S. D. Hamann, *Trans. Faraday Soc.* **55**, 72 (1959); S. D. Hamann and M. Linton, *ibid.* **65**, 2186 (1969).
13. N. C. Holmes *et al.*, *Phys. Rev. Lett.* **55**, 2433 (1985).
14. R. D. Dick, *J. Chem. Phys.* **74**, 4053 (1981).
15. W. J. Nellis *et al.*, *ibid.* **75**, 3055 (1981).
16. A. C. Mitchell *et al.*, in *High-Pressure Science and Technology*, B. Vodar and Ph. Marteau, Eds. (Pergamon, Oxford, 1980), vol. 2, pp. 1048–1050.
17. H. B. Radousky *et al.*, in *Shock Waves in Condensed Matter*, Y. M. Gupta, Ed. (Plenum, New York, 1986), pp. 467–472.
18. M. Ross, in *High Pressure in Research and Industry*, C.-M. Backman, T. Johannisson, L. Tegner, Eds. (Arkitektkopia, Uppsala, 1982), vol. 2, pp. 721–727.
19. D. C. Hamilton, thesis, University of California (1986) (available as Lawrence Livermore National Laboratory report UCRL-53768); D. C. Hamilton *et al.*, *J. Chem. Phys.* **88**, 5042 (1988). A high velocity impactor generates a shock wave by striking the front wall of a cavity containing a liquid specimen. Electrical conductivity is measured by inserting two thin metal foils into the specimen through the rear wall. The specimens are initially insulators. As the shock wave reaches the electrodes, the specimen becomes conductive and current flows. The change in the conductivity of the specimen is detected as a voltage deflection on fast-sweep oscilloscopes. Shock temperature is measured by allowing thermal radiation emitted by the shock front to exit the specimen holder through a window in the rear wall. The emitted light is reflected to a fast multichannel optical pyrometer. EOS data for synthetic Uranus are obtained by measuring the velocities of the impactor and of the resulting shock in the specimen and applying the Rankine-Hugoniot equations.
20. The upper limit of detection is $\gtrsim 100$ (ohm-cm)$^{-1}$. Conductivities larger than 20 (ohm-cm)$^{-1}$ were measured for shocked liquid O_2 [73 ± 10 (ohm-cm)$^{-1}$ at 43 GPa], liquid N_2 [47 ± 6 (ohm-cm)$^{-1}$ at 62 GPa], and liquid benzene [46 ± 9 (ohm-cm)$^{-1}$ at 50 GPa].
21. See, for example, D. J. Stevenson, *Rep. Prog. Phys.* **46**, 555 (1983).
22. F. H. Ree, *J. Chem. Phys.* **81**, 1251 (1984).
23. W. J. Nellis *et al.*, *Phys. Rev. Lett.* **53**, 1661 (1984); H. B. Radousky *et al.*, *ibid.* **57**, 2419 (1986); M. Ross, *J. Chem. Phys.* **86**, 7110 (1987).
24. R. Reichlin *et al.*, *Phys. Rev. Lett.* **55**, 1464 (1985).
25. M. N. Pavlovskii, *Sov. Phys. Solid State* **13**, 741 (1971).
26. W. J. Nellis and A. C. Mitchell, *J. Chem. Phys.* **73**, 6137 (1980).
27. A. K. McMahan and R. LeSar, *Phys. Rev. Lett.* **54**, 1929 (1985).
28. A. K. McMahan, private communication.
29. M. Ross, *Nature* **292**, 435 (1981).

30. We thank D. J. Stevenson and V. N. Zharkov for helpful discussions of their models. We thank A. K. McMahan for use of his unpublished 0 K isotherm for simple cubic O. One of us (M.N.) acknowledges support from the LLNL Branch of the University of California Institute of Geophysics and Planetary Physics and NASA grant NAGW-104. This work was performed under the auspices of the U.S. Department of Energy by the Lawrence Livermore National Laboratory under contract number W-7405-ENG-48, with partial support from the U.S. National Aeronautics and Space Administration under contract W-16, 180.

11 January 1988; accepted 29 March 1988

Hand of *Paranthropus robustus* from Member 1, Swartkrans: Fossil Evidence for Tool Behavior

RANDALL L. SUSMAN

New hand fossils from Swartkrans (dated at about 1.8 million years ago) indicate that the hand of *Paranthropus robustus* was adapted for precision grasping. Functional morphology suggests that *Paranthropus* could have used tools, possibly for plant procurement and processing. The new fossils further suggest that absence of tool behavior was not responsible for the demise of the "robust" lineage. Conversely, these new fossils indicate that the acquisition of tool behavior does not account for the emergence and success of early *Homo*.

THE GENUS *Paranthropus* GENERALLY has been assumed to consist of small-brained, large-toothed early hominids that subsisted on a vegetarian diet (*1*). Stone artifacts found with *Paranthropus* have been attributed to their contemporaries of the genus *Homo* (*2*). With a small brain and a vegetarian diet, it was thought that *Paranthropus* had neither the intellect nor the impetus to engage in tool behavior (*3*, *4*). Further, the lack of tool behavior was thought to have contributed to the eventual extinction of *Paranthropus* in the early middle Pleistocene. Most inferences about *Paranthropus* have come from studies of craniodental remains (*5*). Until now the only postcranial fossils referred to *Paranthropus* are seven bones from Swartkrans (*6*) and four from Kromdraai (*7*).

There are 22 hand bones among 37 new hominid postcranials from Swartkrans (*8*).

Department of Anatomical Sciences, School of Medicine, State University of New York, Stony Brook, NY 11794-8081.